

Article

Incorporation of Antimony Ions in Heptaisobutyl Polyhedral Oligomeric Silsesquioxanes

Stefano Marchesi ¹, Chiara Bisio ^{1,2}, Fabio Carniato ^{1,*} and Enrico Boccaleri ^{3,*}

¹ Dipartimento di Scienze e Innovazione Tecnologica, Università del Piemonte Orientale, Viale Teresa Michel, 11, 15121 Alessandria, Italy; stefano.marchesi@uniupo.it (S.M.); chiara.bisio@uniupo.it (C.B.)

² CNR-SCITEC Istituto di Scienze e Tecnologie Chimiche “G. Natta”, Via C. Golgi 19, 20133 Milano, Italy

³ Dipartimento per lo Sviluppo Sostenibile e la Transizione Ecologica, Università del Piemonte Orientale, Piazza Sant’Eusebio, 5, 13100 Vercelli, Italy

* Correspondence: fabio.carniato@uniupo.it (F.C.); enrico.boccaleri@uniupo.it (E.B.); Tel.: +39-0321360217 (F.C.); +39-0131360264 (E.B.)

Abstract: The direct incorporation of Sb(V) ions into a polycondensed silsesquioxane network based on heptaisobutyl POSS units (Sb(V)-POSSs) through a corner-capping reaction is reported for the first time in this work. As a reference sample, a completely condensed monomeric Sb(III)-POSS was prepared using a similar synthetic protocol. The chemical properties of both Sb-containing POSSs were investigated with different analytical and spectroscopic techniques. The analyses confirm the success of the corner-capping reaction for both samples and indicate that an Sb(V)-POSS sample is characterized by a heterogeneous multimeric arrangement with an irregular organization of POSS cages linked to Sb(V) centers, and has a more complex structure with respect to the well-defined monomeric Sb(III)-POSS.

Keywords: antimony; silsesquioxane; polyhedral oligomeric silsesquioxane; POSS; corner-capping reaction



Citation: Marchesi, S.; Bisio, C.; Carniato, F.; Boccaleri, E.

Incorporation of Antimony Ions in Heptaisobutyl Polyhedral Oligomeric Silsesquioxanes. *Inorganics* **2023**, *11*, 426. <https://doi.org/10.3390/inorganics11110426>

Academic Editors: Torben R. Jensen, Eleonora Aneggi, Hicham Idriss, Roberto Nisticò and Luciano Carlos

Received: 29 September 2023

Revised: 24 October 2023

Accepted: 25 October 2023

Published: 30 October 2023



Copyright: © 2023 by the authors. Licensee MDPI, Basel, Switzerland. This article is an open access article distributed under the terms and conditions of the Creative Commons Attribution (CC BY) license (<https://creativecommons.org/licenses/by/4.0/>).

1. Introduction

Polyhedral oligomeric silsesquioxanes (POSSs) are a unique class of condensed oligomeric organosilicon compounds consisting of an inorganic cage and pendant arms (e.g., H or organic moieties) bound to its apexes. The silicon atoms of the cage are covalently bound to $1/2$ oxygen (*sesqui-*) and hydrogen or hydrocarbon units (*-ane*), globally forming a 3D siloxane (Si-O-Si) skeleton consisting of tetrahedral base units with a generic chemical formula $(\text{RSiO}_{3/2})_n$, where $n = 4\text{--}18$ and R = H or organic substituents [1–4]. Because of their unique nature, they are considered to be excellent models for silica surface sites [5,6] and are very interesting building blocks for the development of hybrid organic–inorganic materials with well-defined physicochemical properties exploitable in many scientific and technological fields [3,7–11].

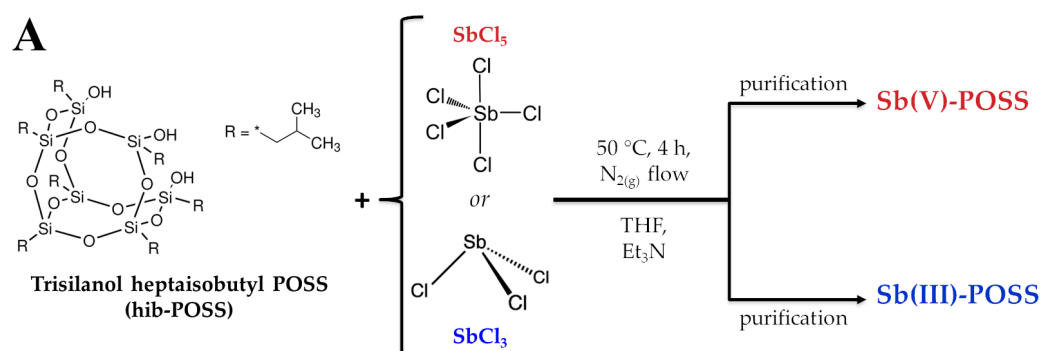
In addition to completely condensed POSSs with a cubic $\text{R}_8\text{Si}_8\text{O}_{12}$ structure and an inorganic cage diameter of 0.5 ± 0.7 nm [1,2], incompletely condensed POSSs containing reactive silanol groups (Si-OH) (e.g., trisilanol $\text{R}_7\text{Si}_7\text{O}_9(\text{OH})_3$) in their core framework [12,13] represent a more interesting class of silsesquioxanes, owing to their ability to bind different functionalities to the inorganic core through reactions with a wide range of organosilanes or heteroelement precursors, the latter in the form of metal halides or alkoxides [13–16]. In the last few years, POSSs have been combined with several elements, from alkali to alkaline earth metals [17–21], metalloids [22–25], transition metals [11,16,25,26], and some lanthanides and actinides [19,27–34]. The construction of metal-containing POSSs [35–37] is achievable through different strategies: (i) a corner-capping reaction, one of the most studied in the literature, in which the Si-OH groups of partially condensed POSSs react with metal ions to generate fully condensed silsesquioxanes [2,38,39]; (ii) a complexation

reaction, where the hydrocarbon groups bonded to the silicon atoms of the cage coordinate the metals [40–42]; and (iii) an interaction between the Si-O^- units of POSS molecules and the metal ions [32,34].

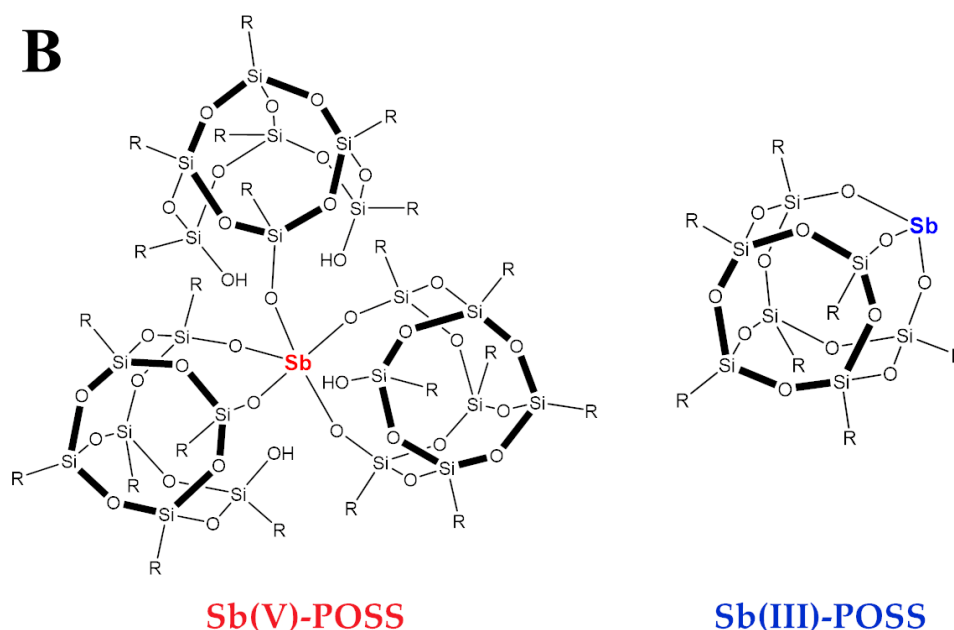
Over the years, several elements in group 15 (pnictogens) of the periodic table have been studied in combination with polysilsesquioxanes and molecular POSSs [43]. Among them, antimony-containing silsesquioxanes are the most investigated, in particular by Feher et al. during the decade 1990–2000 [43–45]. In their work, a series of open-corner cyclohexyl-POSSs were reacted with either (i) a trivalent antimony salt (SbCl_3) through a base-catalyzed corner-capping reaction in benzene at room temperature, giving the correspondent a completely condensed cubic pnictite ester ($c\text{-C}_6\text{H}_{11}$) $_7\text{Si}_7\text{O}_{12}\text{Sb}^{\text{III}}$) [44], or (ii) 1–3 equivalents of the organometallic pentamethylantimony (Me_5Sb), leading to the formation of corresponding mono-, di-, and tri- SbMe_4 -substituted, open-cage silsesquioxides, thus providing an alternative pathway for the preparation of these types of M-POSSs [45]. For Sb(V) -POSS, a monomeric structure with three methylated Sb(V) ions directly attached to three oxygen atoms of the partially condensed silica cage was obtained [45]. Attempted oxidation of Sb(III) to Sb(V) via ozonolysis in cyclohexyl-POSS samples did not lead to any experimental evidence regarding its formation [43,44]. To the best of our knowledge, no attempts have been made to incorporate in a simple synthetic way, without using expensive organic precursor Sb(V) ions directly in the POSS molecular structure.

The inclusion of Sb(V) and Sb(III) ions in POSS structures could be beneficial for the preparation of novel flame-retardant and/or fire-resistant micro- and nano-composite materials. Indeed, silsesquioxanes represent a fascinating 3D hybrid platform for the preparation of polymer/POSS composite materials with tailored fire-related properties (i.e., thermal inertia, ignition temperature, etc.) [17,46–49]. Antimony tri- and pentoxides, along with trihalides and oxyhalides, are well-known for their fire retardancy or resistance properties either in combination with halogenated compounds or blended into suitable composite matrices [50–52] (as halogen-functionalized clays [53] or organoclay combined with plasticizers in thermoplastic polymers [54]), thanks to the establishment of synergistic effects.

Based on these considerations, in this work, we propose the direct incorporation of Sb(V) ions into a polycondensed silsesquioxane matrix through a reaction between trisilanol heptaisobutyl POSS and antimony pentachloride salt in equimolar amounts (Sb(V) -POSS, Scheme 1). The preparation was carried out following a corner-capping reaction procedure [27,43–45,55,56] and realized in anhydrous tetrahydrofuran in the presence of triethylamine. A completely condensed monomeric Sb(III) -POSS was also synthesized with the same procedure as a reference sample.



Scheme 1. Cont.



Scheme 1. (A) Schematic representation of the synthesis procedure of Sb(V)–POSS and Sb(III)–POSS samples. (B) Graphical representation of the structures of Sb(V)–POSS and Sb(III)–POSS.

2. Results and Discussion

A pentavalent antimony-POSS sample (Sb(V)-POSS) was prepared by adapting a corner-capping procedure already used for the preparation of Sb(III)-containing silsesquioxanes [27,43–45,55,56]. The experimental parameters, such as temperature and reaction time, were optimized to achieve a high yield of the materials prepared in this study, while maintaining a stoichiometric ratio of 1:1 between the starting reactants. In detail, the preparation of Sb(V)-POSS was performed in a single step, exploiting a base-assisted corner-capping reaction between the partially condensed trisilanol heptaisobutyl POSS (hib-POSS) and the Sb(V) pentachloride salt (SbCl_5) in an equimolar ratio. The reaction was carried out at 50 °C for 4 h in an inert atmosphere (under N_2 flow). The reaction mixture was carefully purified and a final oily orange product was obtained. The same experimental protocol was used in the preparation of the trivalent Sb(III)-POSS reference.

The chemical composition of the two samples was evaluated by combining elemental CHN and ICP-AES data. For Sb(III)-POSS, the amounts of Sb(III) and carbon corresponded to 1.1 and 31.3 mmol/g, respectively. Considering the organic composition of the POSS unit, it was possible to conclude that each POSS cage was bound to a single Sb(III) ion, with the formation of a fully condensed monomeric structure, in agreement with the results obtained by Feher et al. and Alphazan et al. for the preparation of cyclohexyl-POSS and heptaisobutyl-POSS containing Sb(III) ions through a corner-capping reaction [43–45,55,56]. By contrast, the stoichiometry of Sb(V)-POSS is completely different; the elemental analysis indicated a carbon/Sb(V) molar ratio value of 88.9, thus suggesting a multimeric structure of the sample with three POSS cages coordinated with one Sb(V) center.

The structural features of Sb(V)-POSS were analyzed via X-ray powder diffraction (XRPD) and the diffractogram was compared to that of both Sb(III)-POSS and the open-corner hib-POSS reactant. The X-ray pattern of Sb(V)-POSS (Figure 1c) was characterized by two main broad signals centered at 7 and 19° 2 θ . Compared to the X-ray profile of hib-POSS (Figure 1a), most of the intense and well-resolved crystallographic signals were lost after the reaction. This indicated a loss of order in the arrangement of the silsesquioxane molecules, thus suggesting a mostly irregular rearrangement in the structural network of the POSS cage linked to Sb(V). A similar behavior was also observed for POSS-based polysilsesquioxanes functionalized with Eu^{3+} and/or Tb^{3+} ions and, more generally, in silica-based nanostructures possessing some degree of amorphous components [32,34,57].

Instead, Sb(III)-POSS (Figure 1b) showed a different profile, with the presence of a well-defined reflection at 8.3° 2θ along with several less intense bands at high 2θ values. The presence of these signals suggested a more orderly assembly of the monomeric Sb(III)-POSS with respect to the Sb(V)-POSS sample.

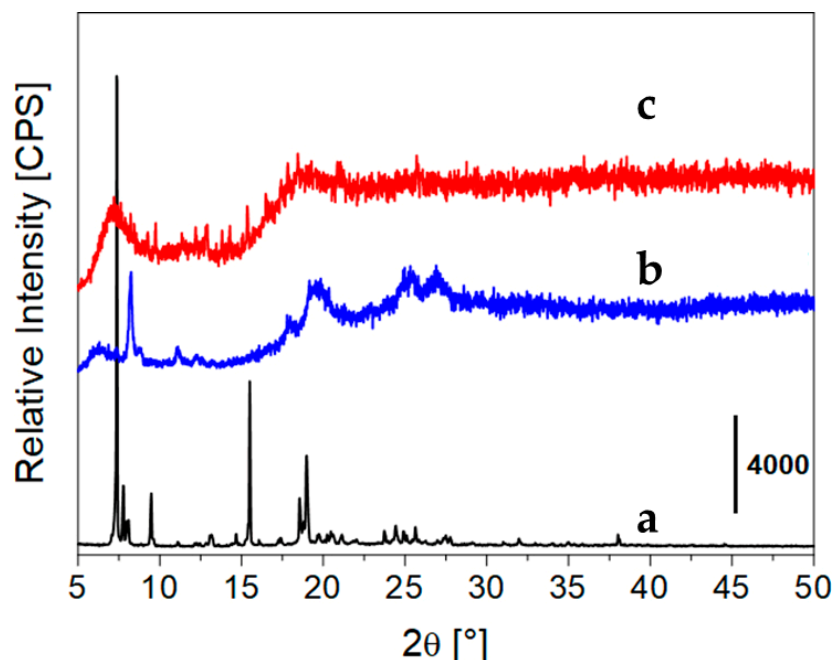


Figure 1. X-ray profiles of hib-POSS (a), Sb(III)-POSS (b), and Sb(V)-POSS (c).

The occurrence of the corner-capping reaction was confirmed through FT-IR spectroscopy by dispersing the solids in a KBr matrix (0.5 wt.%). The vibrational spectrum of Sb(V)-POSS (Figure 2b) was compared to that of both Sb(III)-POSS (Figure 2c) and the reactant hib-POSS (Figure 2a). The IR spectrum of hib-POSS showed two bands at 3250 cm^{-1} and at 890 cm^{-1} , assigned to the stretching of OH and Si-OH groups, respectively. Absorption in the $3000\text{--}2800$ and $1500\text{--}1200\text{ cm}^{-1}$ ranges were attributed to the stretching and bending vibrations of the isobutyl fractions bound to the POSS cage. An intense band centered at 1100 cm^{-1} , due to the vibration modes of the Si-O-Si units, was also detected [58]. After reacting with the metal precursors, the vibrational modes of isobutyl moieties remained unchanged, denoting a preservation of the organic fraction of the POSS unit [27,33,56]. Furthermore, the band attributed to the stretching of Si-O-Si groups appeared to be less intense. This was mainly evident in the spectrum of the Sb(V)-POSS sample. This latter feature is indicative of a local modification of silsesquioxane cage symmetry due to coordination with Sb(III) or Sb(V) ions, consistent with existing literature data on the combination of POSS with several metal centers [29,32,34,59,60]. Finally, the absorptions at 3250 and 890 cm^{-1} were eroded and an intense band at 920 cm^{-1} and 985 cm^{-1} , attributed to the stretching of Si-O-Sb bonds for Sb(III)-POSS and Sb(V)-POSS, respectively, appeared evident in the spectra [56]. In general, this information indicates the success of the corner-capping reaction, with the production of a condensed structure [37,43,61,62]. In the case of the Sb(III)-POSS sample (Figure 2b), the band at approx. 3400 cm^{-1} was assigned to the stretching modes of physisorbed water in the matrix. Signals typical of triethylamine hydrochloride were not present in the IR profiles of either Sb-POSS compound, thus indicating a complete purification of both reaction products.

The XRPD and FT-IR results are well supported by NMR spectroscopy applied to ^1H and ^{29}Si nuclei. Samples were thoroughly dissolved in CDCl_3 for all analyses (see Section 3). The high-resolution ^1H NMR spectrum of Sb(V)-POSS (Figure 3c) was compared to that of both Sb(III)-POSS (Figure 3b) and hib-POSS (Figure 3a). The ^1H NMR spectrum of

hib-POSS showed three main peaks ascribed to the $-CH$ (1.87 ppm), $-CH_2$ (0.61 ppm), and $-CH_3$ (0.98 ppm) protons of the isobutyl groups bound to the POSS cage (Figure 3a) [13,63]. The same profile was also detected for Sb(III)-POSS (Figure 3b), in agreement with previous observations by Feher et al. [44,45] and the 1H NMR spectrum of Sb(V)-POSS (Figure 3c) showed a significant line broadening of the peaks. In addition, a second group of less intense peaks appeared at low ppm (0.68 ppm), which could suggest the presence of two different sets of chemically equivalent methylene groups in different chemical surroundings. The complexity of the structure of Sb(V)-POSS was also confirmed by ^{29}Si NMR data.

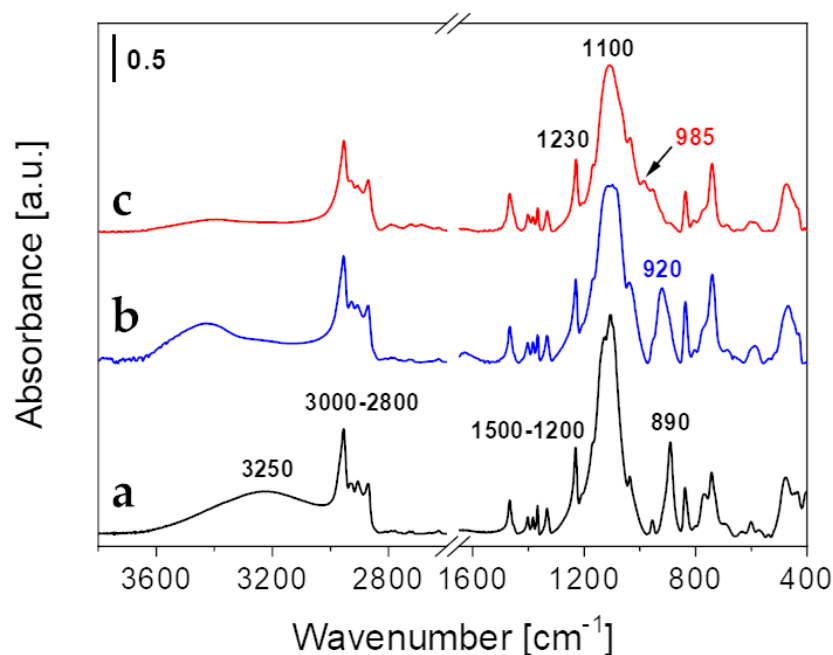


Figure 2. FT-IR spectra of hib-POSS (a), Sb(III)-POSS (b), and Sb(V)-POSS (c) dispersed in a KBr matrix (0.5 wt.%) measured at room temperature (r.t.). Spectra were normalized to the intensity of d isobutyl groups between 1500 and 1200 cm^{-1} .

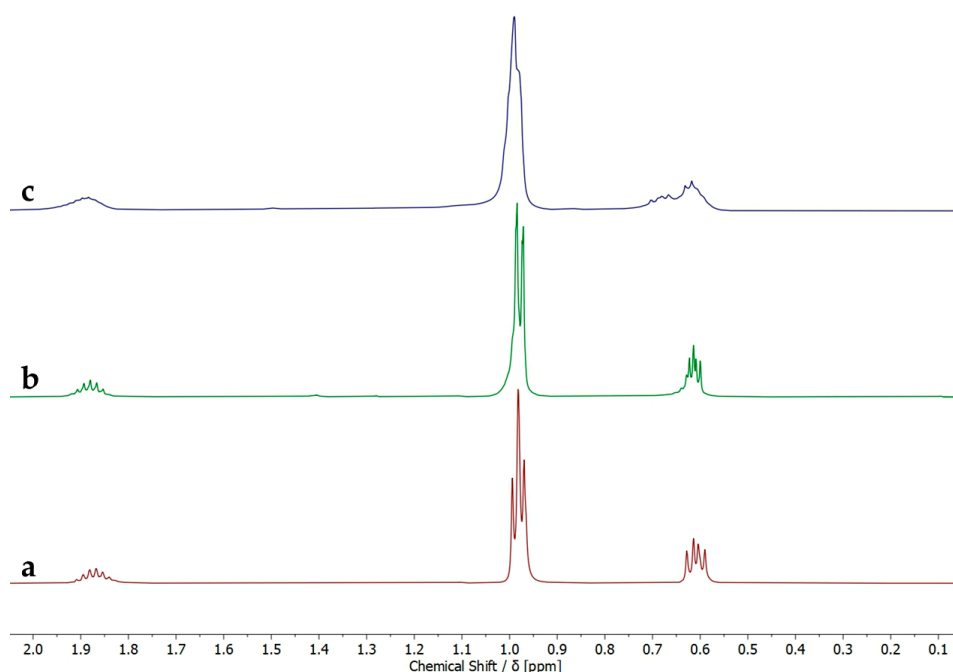


Figure 3. 1H NMR spectra in $CDCl_3$ of hib-POSS (a), Sb(III)-POSS (b), and Sb(V)-POSS (c).

High-resolution ^{29}Si NMR spectra of all compounds provided additional information on the distribution of silicon sites before and after the corner-capping reaction with anti-mony ions. As a general note, the ^{29}Si -NMR spectrum of hib-POSS (Figure 4a) showed three well-defined signals at -58.8 , -67.4 , and -68.6 ppm (3:1:3 ratio). The peak at -58.8 ppm was assigned to the three silicon atoms bound to the hydroxyl groups (Si-OH), whereas the other peaks were ascribed to the remaining silicon sites of the cage [13,27,59,64].

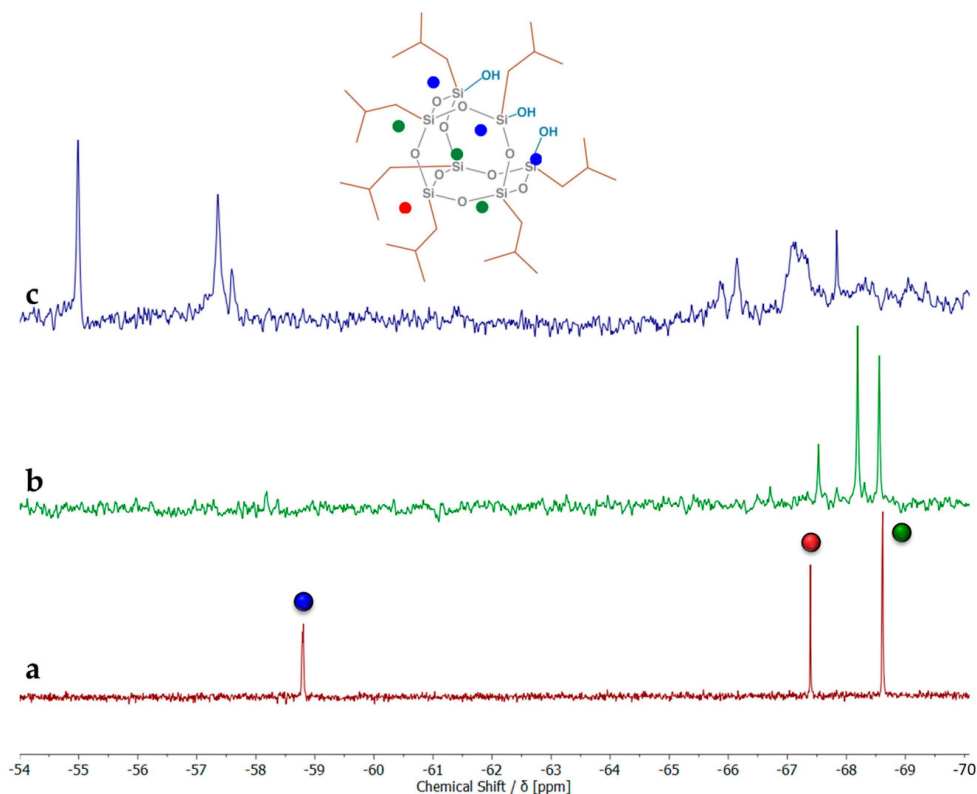


Figure 4. ^{29}Si NMR spectra in CDCl_3 of hib-POSS (a), Sb(III)-POSS (b), and Sb(V)-POSS (c).

The absence of the signal at -58.8 ppm in the ^{29}Si NMR spectrum of Sb(III)-POSS (Figure 4b), along with the presence of a new peak at -68.2 ppm attributed to the Si-O-Sb(III) sites, verified the formation of a fully closed monomeric structure (Figure 5A), in agreement with previous literature studies on the preparation of Sb(III)-doped POSS compounds [44,45,55,56]. Instead, the ^{29}Si NMR spectrum of Sb(V)-POSS (Figure 4c) appeared to be more complicated, with the presence of several peaks. The signals at low ppm (from -65 to -70 ppm) were associated with polycondensed silicon sites in different chemical surroundings, while those between -54 and -60 ppm could be assigned to a fraction of residual silanols (not clearly detectable in the IR spectrum), which were partially involved in coordination with Sb(V) [59]. These results supported the elemental, diffraction, and IR data and confirmed that Sb(V)-POSS is characterized by a more heterogeneous multimetric structure with different stoichiometry, compared to that of monomeric Sb(III)-POSS and to the structures reported in the literature [45]. A hypothetical arrangement of the POSS cages around the Sb(V) site, in analogy to other metal-containing POSS structures previously reported [64,65], is shown in Figure 5B. This representation is based on the Sb/C elemental ratio calculated by CHN analysis and corroborated by the NMR DOSY results. The structures were generated using the Avogadro software (ver. 1.2), optimizing their geometries with the Universal Force Field (UFF).

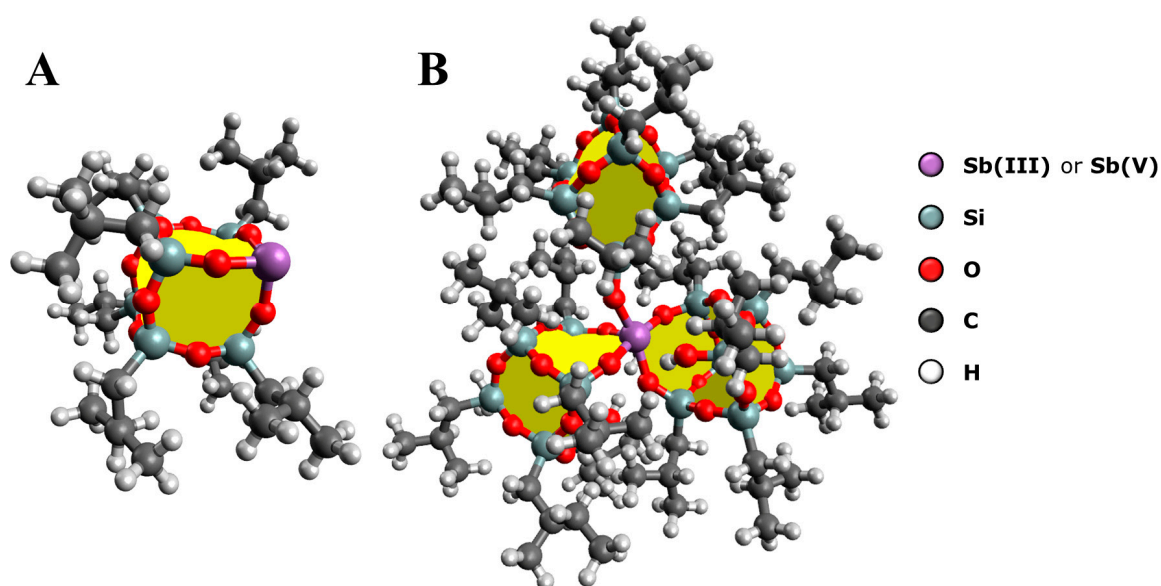


Figure 5. Schematic representation of the structures of Sb(III)–POSS (A) and Sb(V)–POSS (B).

These considerations were also proven with 2D diffusion-ordered spectroscopy (DOSY) ^1H NMR spectra collected for the reference hib-POSS and Sb(V)-POSS samples (Figure 6a and Figure 6b, respectively). The DOSY spectra were recorded in order to determine the molecular translation diffusion coefficients and to estimate the particle size of both samples by applying the Stokes–Einstein Equation (1) defined below:

$$D_t \left[\text{m}^2/\text{s} \right] = \frac{k_b \cdot T}{6\pi \cdot \eta \cdot r} \quad (1)$$

where D_t is the translational diffusion coefficient of the sample analyzed (m^2/s), h is the viscosity of the solvent used in the NMR experiments (CDCl_3 , 0.510 mPa·s), k_b is the Boltzmann constant ($1.380649 \cdot 10^{23}$ J/K), T is the temperature (300 K), and r is the radius of the spheroidal molecule (Å) [66–68].

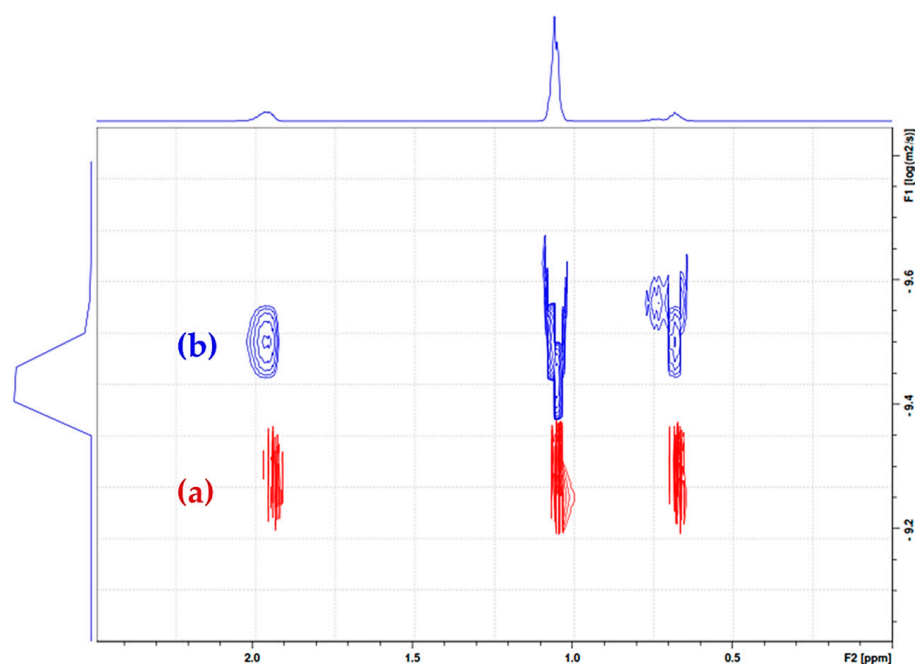


Figure 6. Combined 2D DOSY ^1H NMR spectra in CDCl_3 of hib–POSS (a) and Sb(V)–POSS (b).

The ^1H spectrum of Sb(V)-POSS is reported on the F2 axis and the translational diffusion constants on the F1 axis (in logarithmic scale, m^2/s). For the sake of clarity, we decided to plot only the ^1H NMR spectrum of Sb(V)-POSS on the F2 axis; however, the data in the 2D image are related to both Sb(V)-POSS and hib-POSS samples. The spectra in Figure 6 show a set of three signals for both hib-POSS (Figure 6a) and Sb(V)-POSS (Figure 6b), with a double component visible in the case of the latter. The D_t values extrapolated by the DOSY NMR data were found to be equal to $5.13 \cdot 10^{-10}$ and $3.16 \cdot 10^{-10} \text{ m}^2/\text{s}$ for hib-POSS and Sb(V)-POSS, respectively, corresponding to a particle radius of 8.4 Å for hib-POSS and of 13.6 Å for Sb(V)-POSS. The mean particle size of the Sb(V)-POSS compound was around twice that of the POSS reactant. This result confirmed the existence of a high-molecular-weight multimeric structure for Sb(V)-POSS, compatible with the presence of three POSS units attached to the metal center (Figure 5B). Moreover, a second minor component with a lower diffusion coefficient at 0.68 ppm, already observed in the ^1H NMR spectrum, was also observed (Figure 6b).

3. Materials and Methods

3.1. Reactants

Trisilanol heptaisobutyl silsesquioxane (hib-POSS) was purchased from Hybrid Plastics Inc. (Hattiesburg, MI, USA) and stored at 277 K in the refrigerator. Other chemicals were purchased from Sigma-Aldrich/Merck KGaA (Darmstadt, Germany) and stored at room temperature (r.t.), apart from deuterated chloroform (CDCl_3 , 99.8 atom %D), which was stored at 277 K in the refrigerator. All compounds were used without further purification, unless stated otherwise.

3.2. Materials

3.2.1. Synthesis of Sb(III)-POSS

The completely condensed Sb(III)-doped heptaisobutyl POSS was prepared through a corner-capping reaction, inspired by several synthetic procedures adopted in the literature for the preparation of trivalent antimony-substituted silsesquioxanes [27,43–45,55,56].

In detail, 0.151 g of SbCl_3 (0.66 mmol; $\geq 99.95\%$) was added with vigorous stirring to a solution of 0.500 g of hib-POSS (0.63 mmol) in 30 mL of anhydrous distilled tetrahydrofuran (THF; 0.37 mol; $\geq 99.9\%$) in the presence of 544 mL of triethylamine (Et_3N ; 5.22 mmol; $\geq 99.5\%$). The reaction was carefully purged with nitrogen for 10 min. The temperature was increased to 50 °C and the mixture was stirred for 4 h. Afterwards, the reaction mixture was filtered to remove unreacted reagents and by-products. The filtered solution was evaporated in vacuo and the resulting solid sample was extracted in chloroform (CHCl_3 ; $\geq 99.8\%$) (10 mL + 10 mL of ultrapure water, 3 times); an appropriate amount of sodium sulphate (Na_2SO_4 ; $\geq 99.0\%$) was then used to remove any traces of residual water. The extracted sample was filtered again, evaporated in vacuo, and finally dried overnight in an oven at 50 °C, obtaining a white solid, hereafter named Sb(III)-POSS (yield = 81.7%).

3.2.2. Synthesis of Sb(V)-POSS

Sb(V)-POSS was prepared following the procedure previously described. In detail, 78.5 mL of SbCl_5 (0.66 mmol; $\geq 99.99\%$), carefully dissolved in 10 mL of anhydrous distilled THF (0.12 mol), was added with vigorous stirring to a solution of 0.500 g of hib-POSS (0.63 mmol) in 20 mL of anhydrous distilled THF (0.25 mol) in the presence of 544 mL of Et_3N (5.22 mmol). The reaction was carefully purged with nitrogen for 10 min. The temperature was increased to 50 °C and the mixture was stirred for 4 h. Afterwards, the reaction mixture was filtered to remove unreacted reagents and by-products. The filtered orange solution was evaporated in vacuo and the resulting oily sample was extracted in CHCl_3 ; an appropriate amount of Na_2SO_4 was then used to remove any traces of residual water. The extracted sample was filtered again and evaporated in vacuo, obtaining an oily orange compound, hereafter named Sb(V)-POSS (yield = 62.1%).

3.3. Analytical Methods

Elemental analyses were performed with an Ametek Spectro Genesis EOP Inductively Coupled Plasma Atomic Emission Spectrometer (ICP-AES) (Kleve, Germany) equipped with a cross-flow nebulizer with simultaneous spectrum capture in the 175–770 nm wavelength range. The compounds were mineralized in a mixture of HNO₃ 70% and HF 48% at 373 K for 8 h, and then opportunely diluted in 1 wt.% HNO₃ solutions before analysis.

CHN elemental analyses were performed with an EA3000 CHN Elemental Analyzer (EuroVector, Milano, Italy). Acetanilide, purchased from EuroVector (Milano, Italy), was used as the calibration standard (C % = 71.089, H % = 6.711, N % = 10.363).

X-ray powder diffractograms (XRPDs) were collected on unoriented ground powders using a Bruker D8 Advance Powder Diffractometer (Karlsruhe, Germany), operating in Bragg–Brentano geometry with a Cu anode target equipped with a Ni filter (used as the X-ray source) and a Lynxeye XE-T high-resolution position-sensitive detector. Trio and Twin/Twin optics were mounted on the DaVinci Design modular XRD system. The X-ray tube of the instrument operated with a Cu-K_{α1} monochromatic radiation ($\lambda = 1.54062 \text{ \AA}$), with the current intensity and operative electric potential difference set to 40 mA and 40 kV, respectively, and with automatic variable primary divergent slits and primary and secondary Soller slits of 2.5°. The X-ray profiles were recorded at room temperature in the 5°–50° 2 θ range with a coupled 2 θ – θ method, continuous PSD fast scan mode, time per step (rate or scan speed) of 0.100 s/step, and a 2 θ step size (increment) of 0.01°, with automatic synchronization of the air scatter (or anti-scatter) knife and slits, and a fixed illumination sample set at 15 mm.

Fourier-transform infrared (FT-IR) spectra were collected using a Thermo Electron Corporation FT Nicolet 5700 Spectrometer (Waltham, MA, USA) in the range 4000–400 cm^{−1} with a resolution of 4 cm^{−1}. IR spectra of the solids mixed with potassium bromide (KBr, 0.5 wt.%) pellets were measured in absorbance mode at beam temperature (b.t.). All spectra were normalized to the intensity of the bending modes of isobutyl groups in the 1500–1200 cm^{−1} region.

Then, 1D ¹H (500 MHz), ²⁹Si-{¹H} (99.34 MHz), and 2D DOSY (diffusion-ordered spectroscopy) ¹H Nuclear Magnetic Resonance (NMR) spectra in solution were recorded at 300 K with a Bruker Advance III Spectrometer equipped with a wide bore 11.7 Tesla magnet. The 1D experiments were carried out by dissolving an appropriate amount of each sample (40 mg) in 600 μ L of CDCl₃ and placing them in 5 mm NMR tubes for analyses. A ¹H-decoupling method was used in ²⁹Si experiments to enhance their signals. The 2D DOSY ¹H experiments were performed by dissolving ~55–65 mg of each sample in 550 μ L of CDCl₃. The spectrometer was equipped with a 5 mm double-resonance Z-gradient broadband probe, with the inner coil optimized for the observation of nuclei between ³¹P and ¹⁵N and for ¹⁹F (BBFO), and a Bruker BVT-3000 unit for temperature control. All chemical shifts were reported using the δ [ppm] scale and were externally referenced to tetramethylsilane (TMS) at 0 ppm. Thermogravimetric analysis, TGA, was performed over a Perkin Elmer 7HT apparatus. Analyses were run under dry air with a heating temperature program of 5 °C min^{−1}, from 50 °C to 950 °C. Samples of ca. 10 mg were weighed.

4. Conclusions

In conclusion, we report the direct incorporation of pentavalent antimony ions into a polycondensed silsesquioxane network consisting of heptaisobutyl polyhedral oligomeric silsesquioxane cages as base units. The synthesis of the Sb(V)-POSS compound was accomplished through a corner-capping reaction carried out under mild experimental conditions. A completely condensed heptaisobutyl POSS bound to a single trivalent antimony ion was also prepared as a reference compound. A detailed investigation of the chemical properties of the samples was performed through a multi-technique approach. The ratio between POSS molecules and Sb(V) ions, estimated by CHN and ICP-AES analyses, suggests the average presence of three silsesquioxane cages linked to one Sb(V) ion. Infrared analyses confirmed the successful incorporation of the Sb(V) ions into the inorganic

framework. X-ray powder diffraction studies, combined with 1D ^1H and ^{29}Si NMR spectra, further demonstrate the multimetric nature of the Sb(V)-POSS sample, consisting of an irregular organization of Sb(V)-linked POSS cores in the final structural network. Moreover, the molecular size of Sb(V)-POSS was found to be approx. two times greater than that of trisilanol heptaisobutyl POSS. Future studies will be focused on the application of these Sb-POSSs as flame-retardant additives for polymeric composites.

Author Contributions: Conceptualization, S.M., F.C. and E.B.; methodology, S.M. and F.C.; supervision: E.B.; formal analysis, S.M. and F.C.; investigation, S.M.; data curation, S.M.; writing—original draft preparation, S.M.; writing—review and editing, S.M., C.B., F.C. and E.B. All authors have read and agreed to the published version of the manuscript.

Funding: This research received no external funding.

Data Availability Statement: Not applicable.

Acknowledgments: The authors are fully grateful to Elena Perin for CHN elemental analyses and Chiara Zaccone for ICP-AES elemental analyses.

Conflicts of Interest: The authors declare no conflict of interest.

References

1. Pescarmona, P.P.; Maschmeyer, T. Review: Oligomeric Silsesquioxanes: Synthesis, Characterization and Selected Applications. *Aust. J. Chem.* **2001**, *54*, 583–596. [[CrossRef](#)]
2. Cordes, D.B.; Lickiss, P.D.; Rataboul, F. Recent Developments in the Chemistry of Cubic Polyhedral Oligosilsesquioxanes. *Chem. Rev.* **2010**, *110*, 2081–2173. [[CrossRef](#)] [[PubMed](#)]
3. Kalia, S.; Pielichowski, K. (Eds.) *Polymer/POSS Nanocomposites and Hybrid Materials: Preparation, Properties, Applications*; Springer Series on Polymer and Composite Materials; Springer International Publishing: Cham, Switzerland, 2018; ISBN 978-3-030-02326-3.
4. Laird, M.; Herrmann, N.; Ramsahye, N.; Totée, C.; Carcel, C.; Unno, M.; Bartlett, J.R.; Wong Chi Man, M. Large Polyhedral Oligomeric Silsesquioxane Cages: The Isolation of Functionalized POSS with an Unprecedented $\text{Si}_{18}\text{O}_{27}$ Core. *Angew. Chem. Int. Ed.* **2021**, *60*, 3022–3027. [[CrossRef](#)] [[PubMed](#)]
5. Quadrelli, E.A.; Basset, J.-M. On Silsesquioxanes' Accuracy as Molecular Models for Silica-Grafted Complexes in Heterogeneous Catalysis. *Coord. Chem. Rev.* **2010**, *254*, 707–728. [[CrossRef](#)]
6. Feher, F.J.; Newman, D.A.; Walzer, J.F. Silsesquioxanes as Models for Silica Surfaces. *J. Am. Chem. Soc.* **1989**, *111*, 1741–1748. [[CrossRef](#)]
7. Zhou, H.; Ye, Q.; Xu, J. Polyhedral Oligomeric Silsesquioxane-Based Hybrid Materials and Their Applications. *Mater. Chem. Front.* **2017**, *1*, 212–230. [[CrossRef](#)]
8. Dong, F.; Lu, L.; Ha, C.-S. Silsesquioxane-Containing Hybrid Nanomaterials: Fascinating Platforms for Advanced Applications. *Macromol. Chem. Phys.* **2019**, *220*, 1800324. [[CrossRef](#)]
9. Tunstall-Garcia, H.; Charles, B.L.; Evans, R.C. The Role of Polyhedral Oligomeric Silsesquioxanes in Optical Applications. *Adv. Photonics Res.* **2021**, *2*, 2000196. [[CrossRef](#)]
10. John, L.; Ejfler, J. A Brief Review on Selected Applications of Hybrid Materials Based on Functionalized Cage-like Silsesquioxanes. *Polymers* **2023**, *15*, 1452. [[CrossRef](#)]
11. Calabrese, C.; Aprile, C.; Gruttadauria, M.; Giacalone, F. POSS Nanostructures in Catalysis. *Catal. Sci. Technol.* **2020**, *10*, 7415–7447. [[CrossRef](#)]
12. Blanco, I.; Abate, L.; Bottino, F.A.; Bottino, P. Hepta Isobutyl Polyhedral Oligomeric Silsesquioxanes (Hib-POSS). *J. Therm. Anal. Calorim.* **2012**, *108*, 807–815. [[CrossRef](#)]
13. Ye, M.; Wu, Y.; Zhang, W.; Yang, R. Synthesis of Incompletely Caged Silsesquioxane (T7-POSS) Compounds via a Versatile Three-Step Approach. *Res. Chem. Intermed.* **2018**, *44*, 4277–4294. [[CrossRef](#)]
14. Imoto, H.; Ueda, Y.; Sato, Y.; Nakamura, M.; Mitamura, K.; Watase, S.; Naka, K. Corner- and Side-Opened Cage Silsesquioxanes: Structural Effects on the Materials Properties. *Eur. J. Inorg. Chem.* **2020**, *2020*, 737–742. [[CrossRef](#)]
15. Kaneko, Y.; Coughlin, E.B.; Gunji, T.; Itoh, M.; Matsukawa, K.; Naka, K. Silsesquioxanes: Recent Advancement and Novel Applications. *Int. J. Polym. Sci.* **2012**, *2012*, e453821. [[CrossRef](#)]
16. Lorenz, V.; Edelmann, F.T. Dimeric Silsesquioxanes and Metallasilsesquioxanes—En Route to Large, Welldefined Si-O-Assemblies. *Z. Anorg. Allg. Chem.* **2004**, *630*, 1147–1157. [[CrossRef](#)]
17. Ye, X.; Li, J.; Zhang, W.; Yang, R.; Li, J. Fabrication of Eco-Friendly and Multifunctional Sodium-Containing Polyhedral Oligomeric Silsesquioxane and Its Flame Retardancy on Epoxy Resin. *Compos. B Eng.* **2020**, *191*, 107961. [[CrossRef](#)]
18. Prigyi, N.; Chanmungkalakul, S.; Ervithayasuporn, V.; Yodsinn, N.; Jungsuttiwong, S.; Takeda, N.; Unno, M.; Boonmak, J.; Kiatkamjornwong, S. Lithium-Templated Formation of Polyhedral Oligomeric Silsesquioxanes (POSS). *Inorg. Chem.* **2019**, *58*, 15110–15117. [[CrossRef](#)]

19. Gießmann, S.; Lorenz, V.; Liebing, P.; Hilfert, L.; Fischer, A.; Edelmann, F.T. Synthesis and Structural Study of New Metal-silsesquioxanes of Potassium and Uranium. *Dalton Trans.* **2017**, *46*, 2415–2419. [[CrossRef](#)]
20. Hanssen, R.W.J.M.; Meetsma, A.; van Santen, R.A.; Abbenhuis, H.C.L. Synthesis, Structural Characterization, and Transmetalation Reactions of a Tetranuclear Magnesium Silsesquioxane Complex. *Inorg. Chem.* **2001**, *40*, 4049–4052. [[CrossRef](#)]
21. Lorenz, V.; Fischer, A.; Edelmann, F.T. Silsesquioxane Chemistry, 6: The First Beryllium Silsesquioxane: Synthesis and Structure of $[\text{Cy}_7\text{Si}_7\text{O}_{12}\text{BeLi}]_2 \cdot 2\text{THF}$. *Inorg. Chem. Commun.* **2000**, *3*, 292–295. [[CrossRef](#)]
22. Levitsky, M.M.; Zubavichus, Y.V.; Korlyukov, A.A.; Khrustalev, V.N.; Shubina, E.S.; Bilyachenko, A.N. Silicon and Germanium-Based Sesquioxanes as Versatile Building Blocks for Cage Metallacomplexes. A Review. *J. Clust. Sci.* **2019**, *30*, 1283–1316. [[CrossRef](#)]
23. Kaźmierczak, J.; Kuciński, K.; Stachowiak, H.; Hreczycho, G. Introduction of Boron Functionalities into Silsesquioxanes: Novel Independent Methodologies. *Chem.—Eur. J.* **2018**, *24*, 2509–2514. [[CrossRef](#)]
24. Astakhov, G.S.; Levitsky, M.M.; Zubavichus, Y.V.; Khrustalev, V.N.; Titov, A.A.; Dorovatovskii, P.V.; Smol'yakov, A.F.; Shubina, E.S.; Kirillova, M.V.; Kirillov, A.M.; et al. Cu_6 - and Cu_8 -Cage Sil- and Germanesquioxanes: Synthetic and Structural Features, Oxidative Rearrangements, and Catalytic Activity. *Inorg. Chem.* **2021**, *60*, 8062–8074. [[CrossRef](#)] [[PubMed](#)]
25. Gerritsen, G.; Duchateau, R.; Yap, G.P.A. Boron, Aluminum, and Gallium Silsesquioxane Compounds, Homogeneous Models for Group 13 Element-Containing Silicates and Zeolites. *Organometallics* **2003**, *22*, 100–110. [[CrossRef](#)]
26. Besselink, R.; Venkatachalam, S.; van Wüllen, L.; ten Elshof, J.E. Incorporation of Niobium into Bridged Silsesquioxane Based Silica Networks. *J. Sol-Gel Sci. Technol.* **2014**, *70*, 473–481. [[CrossRef](#)]
27. Marchesi, S.; Carniato, F.; Boccaleri, E. Synthesis and Characterisation of a Novel Europium(III)-Containing Heptaisobutyl-POSS. *New J. Chem.* **2014**, *38*, 2480–2485. [[CrossRef](#)]
28. Willauer, A.R.; Dabrowska, A.M.; Scopelliti, R.; Mazzanti, M. Structure and Small Molecule Activation Reactivity of a Metal-silsesquioxane of Divalent Ytterbium. *Chem. Commun.* **2020**, *56*, 8936–8939. [[CrossRef](#)]
29. Lorenz, V.; Fischer, A.; Gießmann, S.; Gilje, J.W.; Gun'ko, Y.; Jacob, K.; Edelmann, F.T. Disiloxanediolates and Polyhedral Metal-silsesquioxanes of the Early Transition Metals and F-Elements. *Coord. Chem. Rev.* **2000**, *206*, 321–368. [[CrossRef](#)]
30. Marchesi, S.; Carniato, F.; Marchese, L.; Boccaleri, E. Luminescent Mesoporous Silica Built through Self-Assembly of Polyhedral Oligomeric Silsesquioxane and Europium(III) Ions. *ChemPlusChem* **2015**, *80*, 915–918. [[CrossRef](#)]
31. Kumar, B.; Kumar, A.P.; Bindu, P.; Mukherjee, A.; Patra, S. Red Light Emission of POSS Triol Chelated with Europium. *Asian J. Nanosci. Mater.* **2019**, *2*, 244–256. [[CrossRef](#)]
32. Marchesi, S.; Bisio, C.; Boccaleri, E.; Carniato, F. A Luminescent Polysilsesquioxane Obtained by Self-Condensation of Anionic Polyhedral Oligomeric Silsesquioxanes (POSS) and Europium(III) Ions. *ChemPlusChem* **2020**, *85*, 176–182. [[CrossRef](#)]
33. Marchesi, S.; Bisio, C.; Carniato, F. Synthesis of Novel Luminescent Double-Decker Silsesquioxanes Based on Partially Condensed Tetrasilanolphenyl POSS and $\text{Tb}^{3+}/\text{Eu}^{3+}$ Lanthanide Ions. *Processes* **2022**, *10*, 758. [[CrossRef](#)]
34. Marchesi, S.; Miletto, I.; Bisio, C.; Gianotti, E.; Marchese, L.; Carniato, F. Eu^{3+} and Tb^{3+} @ PSQ: Dual Luminescent Polyhedral Oligomeric Polysilsesquioxanes. *Materials* **2022**, *15*, 7996. [[CrossRef](#)] [[PubMed](#)]
35. Levitsky, M.M.; Yalymov, A.I.; Kulakova, A.N.; Petrov, A.A.; Bilyachenko, A.N. Cage-like Metal-silsesquioxanes in Catalysis: A Review. *J. Mol. Catal. A-Chem.* **2017**, *426*, 297–304. [[CrossRef](#)]
36. Lorenz, V.; Edelmann, F.T. Metal-silsesquioxanes. In *Advances in Organometallic Chemistry*; West, R., Hill, A.F., Stone, F.G.A., Eds.; Academic Press: Cambridge, MA, USA, 2005; Volume 53, pp. 101–153.
37. Levitsky, M.M.; Bilyachenko, A.N. Modern Concepts and Methods in the Chemistry of Polyhedral Metal-siloxanes. *Coord. Chem. Rev.* **2016**, *306*, 235–269. [[CrossRef](#)]
38. Pan, G. Polyhedral Oligomeric Silsesquioxane (POSS). In *Physical Properties of Polymers Handbook*; Mark, J.E., Ed.; Springer: New York, NY, USA, 2007; pp. 577–584. ISBN 978-0-387-69002-5.
39. Ward, A.J.; Masters, A.F.; Maschmeyer, T. Metal-silsesquioxanes: Molecular Analogues of Heterogeneous Catalysts. In *Applications of Polyhedral Oligomeric Silsesquioxanes*; Hartmann-Thompson, C., Ed.; Advances in Silicon Science; Springer: Dordrecht, The Netherlands, 2011; pp. 135–166. ISBN 978-90-481-3787-9.
40. Henig, J.; Tóth, É.; Engelmann, J.; Gottschalk, S.; Mayer, H.A. Macrocyclic Gd^{3+} Chelates Attached to a Silsesquioxane Core as Potential Magnetic Resonance Imaging Contrast Agents: Synthesis, Physicochemical Characterization, and Stability Studies. *Inorg. Chem.* **2010**, *49*, 6124–6138. [[CrossRef](#)]
41. Köytepe, S.; Demirel, M.H.; Gültekin, A.; Seçkin, T. Metallo-Supramolecular Materials Based on Terpyridine-Functionalized Polyhedral Silsesquioxane. *Polym. Int.* **2014**, *63*, 778–787. [[CrossRef](#)]
42. Li, Y.; Dong, X.-H.; Zou, Y.; Wang, Z.; Yue, K.; Huang, M.; Liu, H.; Feng, X.; Lin, Z.; Zhang, W.; et al. Polyhedral Oligomeric Silsesquioxane Meets “Click” Chemistry: Rational Design and Facile Preparation of Functional Hybrid Materials. *Polymer* **2017**, *125*, 303–329. [[CrossRef](#)]
43. Murugavel, R.; Voigt, A.; Walawalkar, M.G.; Roesky, H.W. Hetero- and Metal-siloxanes Derived from Silanediols, Disilanol, Silanetriols, and Trisilanol. *Chem. Rev.* **1996**, *96*, 2205–2236. [[CrossRef](#)]
44. Feher, F.J.; Budzichowski, T.A. Heterosilsesquioxanes: Synthesis and Characterization of Group 15 Containing Polyhedral Oligosilsesquioxanes. *Organometallics* **1991**, *10*, 812–815. [[CrossRef](#)]

45. Feher, F.J.; Budzichowski, T.A.; Rahimian, K.; Ziller, J.W. Reactions of Incompletely-Condensed Silsesquioxanes with Pentamethylantimony: A New Synthesis of Metallasilsesquioxanes with Important Implications for the Chemistry of Silica Surfaces. *J. Am. Chem. Soc.* **1992**, *114*, 3859–3866. [[CrossRef](#)]
46. Zhang, W.; Camino, G.; Yang, R. Polymer/Polyhedral Oligomeric Silsesquioxane (POSS) Nanocomposites: An Overview of Fire Retardance. *Prog. Polym. Sci.* **2017**, *67*, 77–125. [[CrossRef](#)]
47. Glodek, T.; Boyd, S.; Mcaninch, I.; Lascala, J. Properties and Performance of Fire Resistant Eco-Composites Using Polyhedral Oligomeric Silsesquioxane (POSS) Fire Retardants. *Compos. Sci. Technol.* **2008**, *68*, 2994–3001. [[CrossRef](#)]
48. Kim, H.-J.; Kwon, Y.; Kim, C.K. Mechanical Property and Thermal Stability of Polyurethane Composites Reinforced with Polyhedral Oligomeric Silsesquioxanes and Inorganic Flame Retardant Filler. *J. Nanosci. Nanotechnol.* **2014**, *14*, 6048–6052. [[CrossRef](#)]
49. Palin, L.; Rombolà, G.; Milanese, M.; Boccaleri, E. The Use of POSS-Based Nanoadditives for Cable-Grade PVC: Effects on Its Thermal Stability. *Polymers* **2019**, *11*, 1105. [[CrossRef](#)] [[PubMed](#)]
50. Weil, E.D.; Levchik, S.V. Commercial Flame Retardancy of Unsaturated Polyester and Vinyl Resins: Review. *J. Fire Sci.* **2004**, *22*, 293–303. [[CrossRef](#)]
51. Li, N.; Xia, Y.; Mao, Z.; Wang, L.; Guan, Y.; Zheng, A. Influence of Antimony Oxide on Flammability of Polypropylene/Intumescent Flame Retardant System. *Polym. Degrad. Stab.* **2012**, *97*, 1737–1744. [[CrossRef](#)]
52. Kim, H.; Kim, J.-S.; Jeong, W. Study on the Flame Retardancy and Hazard Evaluation of Poly(Acrylonitrile-Co-Vinylidene Chloride) Fibers by the Addition of Antimony-Based Flame Retardants. *Polymers* **2022**, *14*, 42. [[CrossRef](#)]
53. Zanetti, M.; Camino, G.; Canavese, D.; Morgan, A.B.; Lamelas, F.J.; Wilkie, C.A. Fire Retardant Halogen–Antimony–Clay Synergism in Polypropylene Layered Silicate Nanocomposites. *Chem. Mater.* **2002**, *14*, 189–193. [[CrossRef](#)]
54. Faryal, S.; Zafar, M.; Nazir, M.S.; Ali, Z.; Hussain, M.; Muhammad Imran, S. The Synergic Effect of Primary and Secondary Flame Retardants on the Improvement in the Flame Retardant and Mechanical Properties of Thermoplastic Polyurethane Nanocomposites. *Appl. Sci.* **2022**, *12*, 10866. [[CrossRef](#)]
55. Alphazan, T.; Díaz Álvarez, A.; Martin, F.; Grampeix, H.; Enyedi, V.; Martinez, E.; Rochat, N.; Veillerot, M.; Dewitte, M.; Nys, J.-P.; et al. Shallow Heavily Doped N⁺⁺ Germanium by Organo-Antimony Monolayer Doping. *ACS Appl. Mater. Interfaces* **2017**, *9*, 20179–20187. [[CrossRef](#)] [[PubMed](#)]
56. Alphazan, T.; Florian, P.; Thieuleux, C. Ethoxy and Silsesquioxane Derivatives of Antimony as Dopant Precursors: Unravelling the Structure and Thermal Stability of Surface Species on SiO₂. *Phys. Chem. Chem. Phys.* **2017**, *19*, 8595–8601. [[CrossRef](#)] [[PubMed](#)]
57. Khouchaf, L.; Boulahya, K.; Das, P.P.; Nicolopoulos, S.; Kis, V.K.; Lábár, J.L. Study of the Microstructure of Amorphous Silica Nanostructures Using High-Resolution Electron Microscopy, Electron Energy Loss Spectroscopy, X-ray Powder Diffraction, and Electron Pair Distribution Function. *Materials* **2020**, *13*, 4393. [[CrossRef](#)] [[PubMed](#)]
58. Carniato, F.; Boccaleri, E.; Marchese, L.; Fina, A.; Tabuani, D.; Camino, G. Synthesis and Characterisation of Metal Isobutylsilsesquioxanes and Their Role as Inorganic–Organic Nanoadditives for Enhancing Polymer Thermal Stability. *Eur. J. Inorg. Chem.* **2007**, *2007*, 585–591. [[CrossRef](#)]
59. Marchesi, S.; Carniato, F.; Palin, L.; Boccaleri, E. POSS as Building-Blocks for the Preparation of Polysilsesquioxanes through an Innovative Synthetic Approach. *Dalton Trans.* **2015**, *44*, 2042–2046. [[CrossRef](#)] [[PubMed](#)]
60. Komagata, Y.; Iimura, T.; Shima, N.; Kudo, T. A Theoretical Study of the Insertion of Atoms and Ions into Titanosilsequioxane (Ti-POSS) in Comparison with POSS. *Int. J. Polym. Sci.* **2012**, *2012*, e391325. [[CrossRef](#)]
61. Jin, L.; Hong, C.; Li, X.; Sun, Z.; Feng, F.; Liu, H. Corner-Opening and Corner-Capping of Mono-Substituted T8 POSS: Product Distribution and Isomerization. *Chem. Commun.* **2022**, *58*, 1573–1576. [[CrossRef](#)]
62. Loman-Cortes, P.; Binte Huq, T.; Vivero-Escoto, J.L. Use of Polyhedral Oligomeric Silsesquioxane (POSS) in Drug Delivery, Photodynamic Therapy and Bioimaging. *Molecules* **2021**, *26*, 6453. [[CrossRef](#)]
63. Alphazan, T.; Mathey, L.; Schwarzwälder, M.; Lin, T.-H.; Rossini, A.J.; Wischert, R.; Enyedi, V.; Fontaine, H.; Veillerot, M.; Lesage, A.; et al. Monolayer Doping of Silicon through Grafting a Tailored Molecular Phosphorus Precursor onto Oxide-Passivated Silicon Surfaces. *Chem. Mater.* **2016**, *28*, 3634–3640. [[CrossRef](#)]
64. Carniato, F.; Boccaleri, E.; Marchese, L. A Versatile Route to Bifunctionalized Silsesquioxane (POSS): Synthesis and Characterisation of Ti-Containing Aminopropylisobutyl-POSS. *Dalton Trans.* **2007**, *1*, 36–39. [[CrossRef](#)]
65. Klein, R.A.; Marinus, C. Synthesis and use of metallized polyhedral oligomeric silsequioxane catalyst compositions. WO2015062759A1, 7 May 2015.
66. Evans, R. The Interpretation of Small Molecule Diffusion Coefficients: Quantitative Use of Diffusion-Ordered NMR Spectroscopy. *Prog. Nucl. Magn. Reson. Spectrosc.* **2020**, *117*, 33–69. [[CrossRef](#)] [[PubMed](#)]
67. Dill, K.A.; Bromberg, S. *Molecular Driving Forces: Statistical Thermodynamics in Chemistry and Biology*; Garland Science: New York, NY, USA, 2003; ISBN 978-0-8153-2051-7.
68. Einstein, A. Über Die von Der Molekularinetischen Theorie Der Wärme Geforderte Bewegung von in Ruhenden Flüssigkeiten Suspendierten Teilchen. *Ann. Phys.* **1905**, *322*, 549–560. [[CrossRef](#)]

Disclaimer/Publisher’s Note: The statements, opinions and data contained in all publications are solely those of the individual author(s) and contributor(s) and not of MDPI and/or the editor(s). MDPI and/or the editor(s) disclaim responsibility for any injury to people or property resulting from any ideas, methods, instructions or products referred to in the content.